

## Vibrational Andreev bound states in magnetic molecules

Denis Golež,<sup>1</sup> Janez Bonča,<sup>1,2</sup> and Rok Žitko<sup>1,2</sup>

<sup>1</sup>Jožef Stefan Institute, Jamova 39, SI-1000 Ljubljana, Slovenia

<sup>2</sup>Faculty of Mathematics and Physics, University of Ljubljana, Jadranska 19, SI-1000 Ljubljana, Slovenia

(Received 9 May 2012; published 27 August 2012)

We predict the existence of vibrational Andreev bound states in deformable magnetic molecules on superconducting surfaces. We discuss the Anderson impurity model with electron-phonon coupling to a realistic anharmonic vibrational mode that modulates the tunneling barrier and show that the vibronic features are spectroscopically most visible near the transition point between the Kondo-screened singlet and the unscreened doublet ground state. We find competing tendencies between phonon hardening due to anharmonicity and softening due to coupling to electrons, contrary to the Anderson-Holstein model and other models with harmonic local phonon mode where the vibrational mode is always softened. In addition, we find that the singlet and doublet many-body states may experience very different effective phonon potentials.

DOI: [10.1103/PhysRevB.86.085142](https://doi.org/10.1103/PhysRevB.86.085142)

PACS number(s): 72.15.Qm, 73.20.Hb, 73.40.Gk, 75.75.—c

Molecules that conduct electrical current,<sup>1–4</sup> when embedded in a junction between two metal electrodes,<sup>5</sup> can become the active element in a circuit, such as a rectifier<sup>6,7</sup> or a memory element.<sup>8</sup> Alternatively, molecules deposited on a metal substrate can be probed by a scanning tunneling microscope to study their diffusion,<sup>9</sup> conformation changes,<sup>10,11</sup> dissociation,<sup>12</sup> and chemical reactions.<sup>13,14</sup> Strong coupling between electronic and vibrational degrees of freedom plays a critical role for the molecule's functional properties.<sup>15,16</sup> The electron-phonon (e-ph) coupling renormalizes the electron-electron (e-e) interaction<sup>17,18</sup> and, if large enough, leads to an effective attractive interaction.<sup>17,19,20</sup> Vibrational modes are detected in the differential conductance spectra as spectral features at characteristic frequencies<sup>21–24</sup> that serve as “molecular fingerprints.”<sup>25–27</sup> In magnetic molecules on normal-metal surfaces, the low-temperature spectra exhibit zero-bias anomalies due to the Kondo screening of the local moment,<sup>28,29</sup> while magnetic molecules adsorbed on superconductors exhibit sharp spectral peaks inside the gap (Andreev bound states, ABSs) due to the competition between the Kondo effect and the electron pairing,<sup>30–35</sup> as has been recently experimentally demonstrated.<sup>36</sup> Since molecules are deformable, the vibrational modes need to be taken into account for a comprehensive description of all features that may occur in the subgap part of the spectrum.

In this work we study a realistic model of a deformable magnetic molecule in contact with a superconductor. The vibrational mode is described using the anharmonic Morse potential<sup>37,38</sup> and the displacement exponentially modulates the tunneling barrier.<sup>39</sup> The anharmonicity is required to remove the unphysical infinite-displacement solution found in the harmonic approximation, while the exponential modulation removes the fluctuating-sign problem of the lowest-order linear coupling; both choices are also closer to reality. We focus on the case of a weakly bound adsorbate with external (center-of-mass) vibrational mode whose energy is comparable with the superconducting gap, so that vibronic features occur inside the gap. In particular, we show that the molecule spectral function features vibrational side peaks in addition to the main ABS peaks. The side peaks are visible for generic model parameters even for moderate, experimentally relevant e-ph coupling strength. Because the peak width

is due only to thermal broadening and experimental noise, this setup permits very precise determination of the phonon frequency renormalization due to the e-ph coupling and the e-e interactions.

We describe the system with the impurity model  $H = H_{\text{band}} + H_{\text{mol}} + H_{\text{osc}} + H_{\text{coup}}$ . Here  $H_{\text{band}} = \sum_{k\sigma} \epsilon_k c_{k,\sigma}^\dagger c_{k,\sigma} + \Delta \sum_{k,\sigma} (c_{k,\sigma}^\dagger c_{-k,-\sigma}^\dagger + \text{H.c.})$ , where  $c_{k,\sigma}$  are the conduction-band electron operators with momentum  $k$ , spin  $\sigma$ , and energy  $\epsilon_k$ , and  $\Delta$  is the superconducting gap.  $H_{\text{mol}} = \epsilon(n_\uparrow + n_\downarrow) + U n_\uparrow n_\downarrow$  is the molecule Hamiltonian, where  $n_\sigma = d_\sigma^\dagger d_\sigma$ ,  $\epsilon$  is the on-site energy, and  $U$  is the e-e repulsion. The quantity  $\delta = \epsilon + U/2$  measures the deviation of the system from the particle-hole (p-h) symmetric point. The displaced molecule feels a realistic Morse potential of the form

$$V_{\text{Morse}} = D_e [1 - \exp(-b\hat{x})]^2, \quad (1)$$

where  $D_e$  is the well depth and  $b$  controls its width. The oscillator Hamiltonian is thus  $H_{\text{osc}} = \hat{p}^2/2m + V_{\text{Morse}}$ . We define the harmonic frequency as  $\omega_0 = b\sqrt{2D_e}/m$ , and the displacement and momentum operators as  $\hat{x} = (\hat{a} + \hat{a}^\dagger)\sqrt{1/2m\omega_0}$  and  $\hat{p} = i(\hat{a}^\dagger - \hat{a})\sqrt{m\omega_0/2}$ , where  $\hat{a}$  and  $\hat{a}^\dagger$  are the phonon ladder operators. The shape of the potential is then fully described by two parameters,  $D_e$  and  $\omega_0$ . The harmonic potential is recovered in the limit  $D_e \rightarrow \infty$ , keeping  $\omega_0$  constant. In the coupling part  $H_{\text{coup}} = V(x) \sum_{k,\sigma} (c_{k,\sigma}^\dagger d_\sigma + \text{H.c.})$ , the tunneling term is exponentially modulated by the molecular displacement:

$$V(x) = V_0 \exp[-g(\hat{a} + \hat{a}^\dagger)],$$

where  $g > 0$  is the e-ph coupling constant. The hybridization strength at zero displacement is characterized by  $\Gamma_0 = \pi\rho V_0^2$ , where  $\rho$  is the density of states in the band in the normal state. In all numerical calculations presented in this work, we set  $U = 1$ ,  $\Delta = 0.04$ , and  $\omega_0 = 0.01$ .

In the absence of e-ph coupling ( $g = 0$ ) and close to the particle-hole symmetric point ( $\delta \sim 0$ ), the ground state of the system depends on the relative values of the Kondo temperature  $T_K$  and the BCS gap  $\Delta$ .<sup>30–32</sup> In the limit  $T_K \gg \Delta$ , the local moment is screened by nonpaired conducting electrons. The ground state is then a spin singlet ( $S$ ) many-body Kondo state.<sup>30</sup> In the opposite limit of  $T_K \ll \Delta$ , the formation

of the Cooper pairs leaves no low-energy electrons available to screen the impurity spin. The ground state is then a spin doublet ( $D$ ) unscreened many-body state. For  $T_K \sim \Delta$ , there is a level crossing between the two different ground states. The subgap part of the spectral function for  $g = 0$  has generically two peaks, located symmetrically with respect to the Fermi level (here fixed at  $\omega = 0$ ). These features, often referred to as the Andreev bound states or Shiba states, correspond to the transitions between the  $S$  and  $D$  many-body states. These states are “bound” in the sense that they correspond to excitations below the continuum of quasiparticle states and that the corresponding spectral weight is localized around the impurity site. The transitions can occur either by injecting an electron ( $\omega > 0$  peak) or by removing it ( $\omega < 0$  peak). Away from the p-h symmetric point, the weights of these two peaks are different.<sup>35</sup> Their spectral weights go to zero as the  $S$ - $D$  energy difference tends toward  $\Delta$  in both small- $\Gamma$  ( $T_K \ll \Delta$ ) and large- $\Gamma$  ( $T_K \gg \Delta$ ) hybridization limits and is maximal near the  $S$ - $D$  level crossing,<sup>34</sup> which is signaled by the crossing of the subgap peaks in the spectrum.<sup>32,36</sup>

We now consider the effect of the e-ph coupling ( $g > 0$ ) on the subgap states. For small coupling the hybridization is renormalized as  $\Gamma_0 \rightarrow \tilde{\Gamma} = \Gamma(g, \langle x \rangle)$ , where  $\langle x \rangle$  is the expectation value of the displacement that is negative (the molecule approaches the surface) and linear in  $g$  [see Figs. 3(g)–3(i)], thus the enhancement of the hybridization is approximately quadratic. For large coupling this mean-field approximation is no longer accurate, but the trend toward stronger effective  $\Gamma$  remains. In addition, if the phonon frequency is smaller than the BCS gap,  $\omega_0 < \Delta$ , entirely new features (vibronic ABS side peaks) appear in the subgap part of the molecule spectral function, as we show in the following.

The full problem is solved using the numerical renormalization group<sup>40,41</sup> with extensions for superconducting bands.<sup>30–32</sup> This technique treats all interactions (e-ph coupling, e-e repulsion, BCS pairing) on equal footing. The calculations have been performed for the discretization parameter  $\Lambda = 4$  and are fully converged with respect to the phonon cutoff and the number of states kept in the truncation.

We first consider the evolution of the subgap states as a function of the hybridization strength  $\Gamma_0$ , keeping the e-ph coupling  $g$  constant; see Fig. 1(a). This is motivated by the experimental realization of the singlet-doublet crossing, which is tuned by small changes in the molecule-substrate coupling.<sup>36</sup> The calculation has been performed for generic parameter values, in particular away from the p-h symmetric point. The level crossing between the doublet and singlet ground states  $D0$  and  $S0$  occurs at  $\Gamma_0 = \Gamma_{0c}$ . All other excited subgap states, one series of  $D$  states ( $D1, D2, \dots$ ), and another of  $S$  states ( $S1, S2, \dots$ ), are phonon induced. For a harmonic potential and very weak e-ph coupling, these vibronic states would form ladders with equidistant spacing  $\omega_0$ . For the anharmonic Morse potential, however, the exact solution for the vibrational energy levels includes a quadratic correction term<sup>37</sup> and, furthermore, the effective energy spacing is renormalized by the e-ph coupling;<sup>39,42–44</sup> see also Figs. 3(d)–3(f).

The subgap part of the spectral function, Fig. 1(b), demonstrates that in addition to the main spectral peak ( $S0$ - $D0$  transitions), other phonon-induced side peaks ( $S0$ - $D1$ ,  $D0$ - $S1$ , etc., transitions) are also present and have sufficient spectral

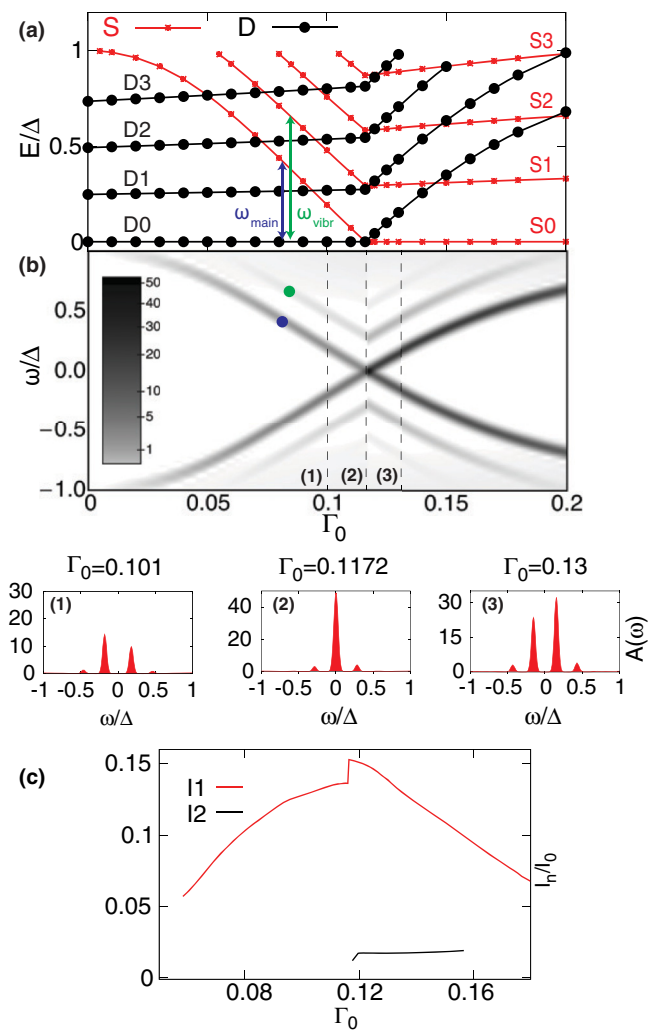


FIG. 1. (Color online) (a) Energy of the subgap singlet ( $S$ ) and doublet ( $D$ ) states as a function of the hybridization strength  $\Gamma_0$ . (b) Subgap part of the spectral function. Subfigures show cross sections at particular values of  $\Gamma_0$ , indicated by dashed lines. (c) Visibility of the first and second vibronic side peaks. Parameters are  $g = 0.05$ ,  $D_e = 0.5$ , and  $\delta = 0.1$ .

weight to be observable. The subfigures, Figs. 1(b1)–1(b3), show spectral curves at three characteristic parameter regimes; first side peaks are clearly resolved in all cases. The ratio between the spectral weight of the side peaks and that of the main ABS peaks (i.e., the visibility), Fig. 1(c), is maximal near the level crossing. We also find that the visibility is largest at the p-h symmetric point ( $\delta = 0$ ) and is reduced somewhat away from it (results not shown).

Alternatively, the  $S$ - $D$  transition can be induced by increasing the e-ph coupling  $g$  at fixed  $\Gamma_0$ ; see Fig. 2. The vibrational excited states exhibit an unexpected feature: with increasing e-ph coupling, the effective phonon frequency increases (the phonon mode hardens). The renormalization of the phonon frequency has been noted in previous studies of impurity models with vibration modes,<sup>39,42–44</sup> where the phonon mode softens. This is the case both for the coupling to charge (Anderson-Holstein model) and for the coupling to the center-of-mass modes. The phonon hardening is a

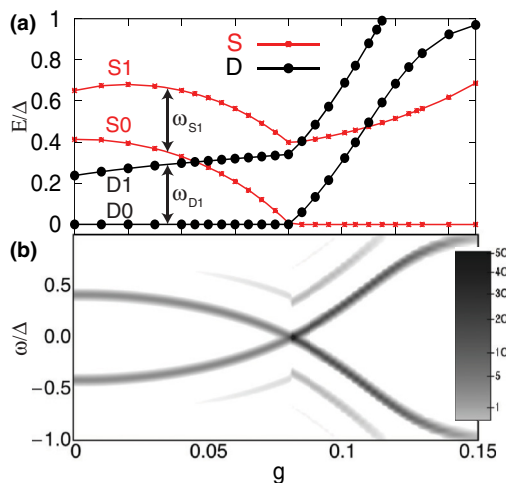


FIG. 2. (Color online) (a) Energy of the subgap singlet ( $S$ ) and doublet ( $D$ ) states as a function of the electron-phonon coupling  $g$ . (b) Subgap part of the spectral function. Parameters are  $\Gamma_0 = 0.1$ ,  $D_e = 0.1$ , and  $\delta = 0$ .

characteristic feature of the anharmonic potential and results from the displacement of the oscillator to the part of the potential with higher second derivative, while the softening results from the electron tunneling fluctuations<sup>45</sup> and occurs generically. Both tendencies are present in our model and the dominant effect depends on the value of the parameter  $D_e$ .

In order to compare the degree of the anharmonicity, the bare (nonrenormalized) potential profiles are shown in the top panel of Fig. 3. In Figs. 3(a)–3(c) the energy dependence of the Andreev states shows the  $S$ - $D$  transition as a function of the e-ph coupling  $g$  for different values of  $D_e$ . The renormalized phonon frequencies, Figs. 3(d)–3(f), indicate that for  $D_e = 0.1$ , the potential is strongly anharmonic and the phonon mode hardens, while for  $D_e = 5$ , in the harmonic limit, it softens. We also observe remarkably large differences in the  $D$  and  $S$  sectors, which are the most pronounced for intermediate anharmonicity where, as a function of  $g$ , the phonon mode softens in the  $D$  sector, while it hardens in the  $S$  sector [see Fig. 3(e)]. The deformation of the molecules as a function of  $g$  is shown in Figs. 3(g)–3(i) (notice that the horizontal ranges are different). In the harmonic limit the e-ph coupling leads to unphysically strong deformation already at small values of  $g$ , while for anharmonic potential, the displacement of the molecule is constrained by the repulsive part of the Morse potential. The insets represent the fluctuations of the displacement,  $\delta x = (\langle x^2 \rangle - \langle x \rangle^2)^{1/2}$ , which in the harmonic limit strongly increase at the transition and then rapidly drop at higher  $g$ , while for strongly anharmonic potential they decrease monotonously and there is no enhancement at the transition. Independent of the anharmonicity parameter  $D_e$ , the visibility grows with increasing e-ph coupling for  $g < g_c$ ; see Figs. 3(j)–3(l). For larger e-ph coupling the visibility starts to decrease, since the energy difference between the ground state and the side peak states approaches the BCS gap.<sup>34</sup> The maximum of the visibility thus generically occurs near the  $S$ - $D$  transition. The visibility is larger for high  $D_e$  values, i.e., in the harmonic limit.

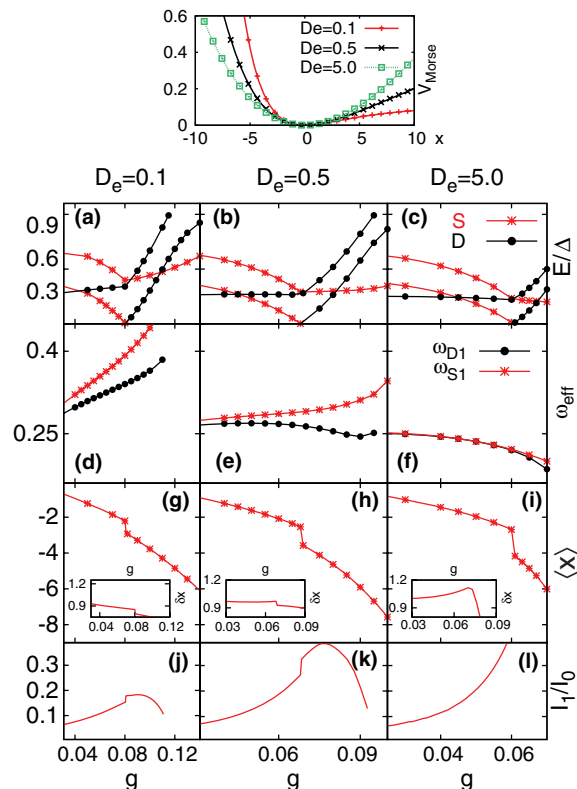


FIG. 3. (Color online) Top panel: bare (nonrenormalized) Morse potential for different parameters of the anharmonicity. Bottom panel: (a)–(c) Energy of the subgap singlet ( $S$ ) and doublet ( $D$ ) states versus electron-phonon coupling  $g$  for different parameters of the anharmonicity. Parameters:  $\Gamma_0 = 0.1$ ,  $\delta = 0$ . (d)–(f) Effective phonon frequencies of  $D$  and  $S$  states. (g)–(i) Displacement and fluctuations (insets) of the displacement. (j)–(l) Visibility of first vibronic side peak.

The oscillator distribution functions  $\rho(x)$  and the effective potentials  $V_{\text{eff}}(x)$ , calculated using the reduced phonon density matrix,<sup>46</sup> are shown in Fig. 4. The minimum of the effective potential is significantly shifted due to the e-ph coupling to its new equilibrium position and we find that the effective potential is not the same for  $S$  and  $D$  states. This implies that the oscillator parameters are renormalized differently in the two spin sectors due to different electron tunneling rates in the unscreened  $D$  and Kondo screened  $S$  many-body states. In the weak coupling (small- $g$ ) regime the effect of the phonons on the subgap part of the spectral function can be understood using the Frank-Condon principle,<sup>47</sup> which states that the transition between the vibrational states is more likely to happen if the vibrational wave functions overlap more significantly. The overlap of the effective vibronic part of the wave functions,  $\phi(x) = \sqrt{\rho(x)}$ , is proportional to the transition probability between the states. For the lowest-lying singlet  $S0$  and doublet  $D0$  states, and the excited singlet  $S1$  and doublet  $D1$  states, the overlaps are represented in Fig. 4(d). Within the Franck-Condon approximation the overlap ratio  $|\langle S0|D1 \rangle|^2 / |\langle S0|D0 \rangle|^2$  is proportional to the visibility and provides good agreement with the actual values, Fig. 3(j),

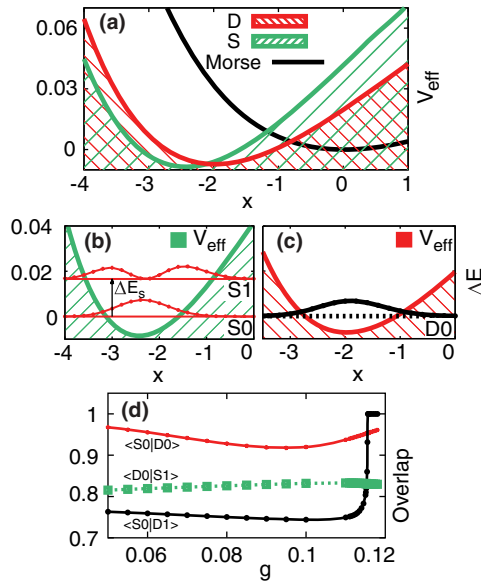


FIG. 4. (Color online) (a) Effective (renormalized) potential of  $S$  and  $D$  subgap states and bare (nonrenormalized) Morse potential. (b),(c) Oscillator distribution  $\rho(x)$  for ABS in the effective potential for  $S$  and  $D$  states. The probability is not normalized. (d) Overlap of the phonon part of the wave function between different subgap states. Parameters are  $\Gamma_0 = 0.1$ ,  $D_e = 0.1$ ,  $\delta = 0$ .

for small electron-phonon couplings  $g$ . However, since the Franck-Condon principle is based on the Born-Oppenheimer

approximation, polaronic effects are neglected and therefore it cannot explain the features in the spectral function for e-ph interaction close to or beyond the level crossing. The sudden increase in the overlap between the  $S_0$  and  $D_1$  states for  $g \approx 0.115$  coincides with the transition of the  $D_1$  state into the continuum, where the excited  $D_1$  state strongly mixes with the direct product states consisting of the  $S_0$  state and an additional continuum low-energy quasiparticle, thus its vibrational properties are essentially those of the  $S_0$  state, which explains the perfect overlap.

We have shown that due to the deformability of the molecule additional vibronic states occur inside the BCS gap, which are clearly visible in the subgap part of the spectral function. We find that generically the intensity of the side peak reaches a maximum close to the ground-state level crossing, but that the peak intensity depends on the system parameters: it increases near the particle-hole symmetric point, for large  $D_e$ , and for large e-ph coupling  $g$ . The increase in the visibility for weak e-ph coupling can be described using the Franck-Condon principle.

To test the predictions of this work, we propose as candidate systems planar macrocyclic molecules which form coordination complexes with weak metal-ligand bonds, so that the magnetic ions support low frequency “rattling” modes, while appropriate surfaces are elemental BCS superconductors.

The authors acknowledge discussions with J. Mravlje, T. Rejec, A. Ramšak, and P. Prelovšek, and the support from the Slovenian Research Agency (ARRS) under Program P1-0044.

- <sup>1</sup>L. A. Bumm, J. J. Arnold, M. T. Cygan, T. D. Dunbar, T. P. Burgin, L. Jones II, D. L. Allara, J. M. Tour, and P. S. Weiss, *Science* **271**, 1705 (1996).
- <sup>2</sup>A. Nitzan, *Annu. Rev. Phys. Chem.* **52**, 681 (2001).
- <sup>3</sup>H. Song, M. A. Reed, and T. Lee, *Adv. Mater.* **23**, 1583 (2011).
- <sup>4</sup>N. A. Zimbovskaya and M. R. Pederson, *Phys. Rep.* **509**, 1 (2011).
- <sup>5</sup>M. A. Reed, C. Zhou, C. J. Muller, T. P. Burgin, and J. M. Tour, *Science* **278**, 252 (1997).
- <sup>6</sup>A. Aviram and M. A. Ratner, *Chem. Phys. Lett.* **29**, 277 (1974).
- <sup>7</sup>I. Díez-Pérez, J. Hihath, Y. Lee, L. Yu, L. Adamska, M. A. Kozhushner, I. I. Oleynik, and N. Tao, *Nat. Chem.* **1**, 635 (2009).
- <sup>8</sup>J. Chen, M. A. Reed, A. M. Rawlett, and J. M. Tour, *Science* **286**, 1550 (1999).
- <sup>9</sup>M. Schunack, T. R. Linderoth, F. Rosei, E. Laegsgaard, I. Stensgaard, and F. Besenbacher, *Phys. Rev. Lett.* **88**, 156102 (2002).
- <sup>10</sup>F. Moresco, G. Meyer, K. H. Rieder, H. Tang, A. Gourdon, and C. Joachim, *Phys. Rev. Lett.* **86**, 672 (2001).
- <sup>11</sup>Z. J. Donhauer, B. A. Mantooth, K. F. Kelly, L. A. Bumm, J. D. Monnell, J. J. Stapleton, D. W. Price Jr., A. M. Rawlett, D. L. Allara, J. M. Tour, and P. S. Weiss, *Science* **292**, 2303 (2001).
- <sup>12</sup>B. C. Stipe, M. A. Rezaei, W. Ho, S. Gao, M. Persson, and B. I. Lundqvist, *Phys. Rev. Lett.* **78**, 4410 (1997).
- <sup>13</sup>W. Ho and H. J. Lee, *Science* **286**, 1719 (1999).
- <sup>14</sup>S.-W. Hla, L. Bartels, G. Meyer, and K.-H. Rieder, *Phys. Rev. Lett.* **85**, 2777 (2000).
- <sup>15</sup>M. Galperin, A. Nitzan, and M. A. Ratner, *Phys. Rev. B* **74**, 075326 (2006).
- <sup>16</sup>R. Leturcq, C. Stampfer, K. Inderbitzin, L. Durrer, C. Hierold, E. Mariani, M. Schultz, F. Von Oppen, and K. Ensslin, *Nat. Phys.* **5**, 327 (2009).
- <sup>17</sup>P. S. Cornaglia, H. Ness, and D. R. Grempel, *Phys. Rev. Lett.* **93**, 147201 (2004).
- <sup>18</sup>P. S. Cornaglia, G. Usaj, and C. A. Balseiro, *Phys. Rev. B* **76**, 241403 (2007).
- <sup>19</sup>P. S. Cornaglia, D. R. Grempel, and H. Ness, *Phys. Rev. B* **71**, 075320 (2005).
- <sup>20</sup>J. Mravlje, A. Ramšak, and T. Rejec, *Phys. Rev. B* **72**, 121403(R) (2005).
- <sup>21</sup>R. C. Jaklevic and J. Lambe, *Phys. Rev. Lett.* **17**, 1139 (1966).
- <sup>22</sup>H. Park, J. Park, A. K. L. Lim, E. H. Anderson, A. P. Alivisatos, and P. L. McEuen, *Nature (London)* **407**, 57 (2000).
- <sup>23</sup>N. Lorente and M. Persson, *Phys. Rev. Lett.* **85**, 2997 (2000).
- <sup>24</sup>L. H. Yu, Z. K. Keane, J. W. Ciszek, L. Cheng, M. P. Stewart, J. M. Tour, and D. Natelson, *Phys. Rev. Lett.* **93**, 266802 (2004).
- <sup>25</sup>B. C. Stipe, M. A. Rezaei, and W. Ho, *Science* **280**, 1732 (1998).
- <sup>26</sup>B. C. Stipe, M. A. Rezaei, and W. Ho, *Phys. Rev. Lett.* **82**, 1724 (1999).
- <sup>27</sup>W. Ho, *J. Chem. Phys.* **117**, 11033 (2002).
- <sup>28</sup>A. Zhao, Q. Li, L. Chen, H. Xiang, W. Wang, S. Pan, B. Wang, X. Xiao, J. Yang, J. G. Hou, and Q. Zhu, *Science* **309**, 1542 (2005).
- <sup>29</sup>G. D. Scott and D. Natelson, *ACS Nano* **4**, 3560 (2010).

- <sup>30</sup>K. Satori, H. Shiba, O. Sakai, and Y. Shimizu, *J. Phys. Soc. Jpn.* **61**, 3239 (1992).
- <sup>31</sup>O. Sakai, Y. Shimizu, H. Shiba, and K. Satori, *J. Phys. Soc. Jpn.* **62**, 3181 (1993).
- <sup>32</sup>T. Yoshioka and Y. Ohashi, *J. Phys. Soc. Jpn.* **69**, 1812 (2000).
- <sup>33</sup>A. Oguri, Y. Tanaka, and A. C. Hewson, *J. Phys. Soc. Jpn.* **73**, 2494 (2004).
- <sup>34</sup>J. Bauer, A. Oguri, and A. C. Hewson, *J. Phys.: Condens. Matter* **19**, 486211 (2007).
- <sup>35</sup>T. Hecht, Ph.D. thesis, Ludwig-Maximilians-Universität München, Munich, 2008.
- <sup>36</sup>K. J. Franke, G. Schulze, and J. I. Pascual, *Science* **332**, 940 (2011).
- <sup>37</sup>P. M. Morse, *Phys. Rev.* **34**, 57 (1929).
- <sup>38</sup>J. Koch and F. von Oppen, *Phys. Rev. B* **72**, 113308 (2005).
- <sup>39</sup>J. Mravlje and A. Ramšak, *Phys. Rev. B* **78**, 235416 (2008).
- <sup>40</sup>K. G. Wilson, *Rev. Mod. Phys.* **47**, 773 (1975).
- <sup>41</sup>R. Bulla, T. Costi, and T. Pruschke, *Rev. Mod. Phys.* **80**, 395 (2008).
- <sup>42</sup>A. C. Hewson and D. Meyer, *J. Phys.: Condens. Matter* **14**, 427 (2002).
- <sup>43</sup>D. Meyer, A. C. Hewson, and R. Bulla, *Phys. Rev. Lett.* **89**, 196401 (2002).
- <sup>44</sup>G. S. Jeon, T.-H. Park, and H.-Y. Choi, *Phys. Rev. B* **68**, 045106 (2003).
- <sup>45</sup>C. A. Balseiro, P. S. Cornaglia, and D. R. Grempel, *Phys. Rev. B* **74**, 235409 (2006).
- <sup>46</sup>A. C. Hewson and J. Bauer, *J. Phys.: Condens. Matter* **22**, 115602 (2010).
- <sup>47</sup>E. U. Condon, *Phys. Rev.* **32**, 858 (1928).